Chin. Geogra. Sci. 2012 Vol. 22 No. 4 pp. 450–461
doi: 10.1007/s11769-012-0551-z
www.springerlink.com/content/1002-0063

Holocene Climate Cycles in Northwest Margin of Asian Monsoon

LI Yu, WANG Nai′ang, LI Zhuolun, ZHOU Xuehua, ZHANG Chengqi
(*College of Earth and Environmental Sciences, Center for Hydrologic Cycle and Water Resources in Arid Region, Lanzhou University, Lanzhou 730000, China*)

Abstract: In the mid-latitude regions of the Asian continent, Zhuye Lake is located in the northwest margin of the Asian monsoon, where the modern climate is affected by the Asian monsoon and Westerlies. In this study, we investigated the absolutely dated Holocene records in Zhuye Lake for detecting the Holocene climate cycles. Totally, 14 ^{14}C dates and 6 optically simulated luminescence (OSL) dates are obtained from the QTH01 and QTH02 sections. The proxies of grain-size, total organic carbon content (TOC), C/N and $\delta^{13}C$ are used for wavelet analysis, and the results show obvious ~256, ~512 and ~1024-year climate cycles, which are consistent with the Holocene millennial and centennial scale climate cycles in the typical Asian summer monsoon domain. In different parts of the Zhuye Lake, the Holocene sediments show variable climate cycles that are affected by the lake basin topography. In the Zhuye Lake, the Holocene climate cycles are mainly correlated with the solar-related Asian summer monsoon variability and the North Atlantic ice-rafting events.

Keywords: Holocene; climate cycle; Asian monsoon; wavelet analysis; Zhuye Lake

Citation: Li Yu, Wang Nai′ang, Li Zhuolun, Zhou Xuehua, Zhang Chengqi, 2012. Holocene climate cycles in northwest margin of Asian monsoon. *Chinese Geographical Science*, 22(4): 450–461. doi: 10.1007/s11769-012-0551-z

1 Introduction

The investigation of past climate change can understand the past environment of Earth and predict the climate in the future. To study past climate change, it is important to examine climate cycles, and there are variable climate cycles on different time scales, such as orbital, millennial, centennial and decadal scales (Sonnet and Suess, 1984; Stuiver and Braziunas, 1993; Palus *et al*., 2007). In the Greenland ice cores, the Dansgaard-Oeschger events have been detected during the Last Glacial, and detailed spectral analysis of the Greenland ice core $\delta^{18}O$ record has proven a ~1500-year cycle, that is interpreted as the preferred recurrence time of Dansgaard-Oeschger events (Dansgaard *et al*., 1993; Grootes *et al*., 1993; Yiou *et al*., 1997). Bond *et al*. (1997) argued for a cyclicity close to 1470 ± 500 years in the North Atlantic region during the Holocene, primarily from fluctuations in ice-rafted debris. In their view, the Dansgaard-Oeschger events of the Last Glacial conform to a 1500-year pattern, as do some climate events of later eras, like the Little Ice Age, the 8.2 kyr event, and the start of the Younger Dryas. Bond *et al*. (2001) theorized that variations in solar activity, the appearance of sunspots and changes in the emission of solar radiation, might be driving 1500-year-cycles of cold events in Northern Hemisphere climate. High-resolution analyses of lake sediment from southwestern Alaska revealed cyclic variations in climate and ecosystems during the Holocene and these variations also occurred with periodicities similar to those of solar activity (Feng *et al*., 2003). Solar variability is often considered likely to be responsible for centennial and millennial scale Holocene climate cycles, yet the origin of the centennial and millennial scale cycles during the Holocene remains a mystery (Rahmstorf, 2003). Therefore, investigating Holocene climate cycles in different parts of the earth is good for understanding the mechanism of Holocene

Received date: 2011-07-20; accepted date: 2011-11-22
Foundation item: Under the auspices of National Natural Science Foundation of China (No. 41001116), Fundamental Research Funds for the Central Universities (No. LZUJBKY-2010-99)
Corresponding author: LI Yu. E-mail: liyu@lzu.edu.cn

climate cycles. In the Asian monsoon domain, Gupta *et al*. (2003) reported that a Holocene monsoon proxy record revealed several intervals of weak summer monsoon that coincide with cold periods documented in the North Atlantic region in the Arabian Sea, which suggested that the link between the North Atlantic Ocean and the Asian monsoon is a persistent aspect of global climate. From the inland of the Asian monsoon domain, the cave records show the absolutely dated and high-resolution records. The solar activity induced multi-decadal monsoon precipitation variations can be detected in Oman by stalagmite records study (Fleitmann *et al*., 2003). Wang *et al*. (2005) found that the Holocene Asian monsoon precipitation was linked to the solar changes and the North Atlantic climate. In monsoonal China, the Holocene lake and peat records also indicated solar-related Asian summer monsoon cycles (Liu *et al*., 2000; Xian *et al*., 2006). In East Asia, the monsoonal climate has different impacts for different parts of China, and the climate cycles may vary from the locations; therefore, it is also important to detect the Holocene climate cycles in arid China, where the climate is sensitive to the Asian monsoon.

The Zhuye Lake is located in arid regions of the Asian continent. The palynological and geochemical proxies showed the Holocene long-term environmental changes (Li *et al*., 2009a; 2009b; Long *et al*., 2010). The results of these studies indicated the mid-Holocene Climatic Optimum and reconstructed the long-term lake level evolution. However, little attention was paid to the Holocene climate cycles. In addition, previous studies have examined the Holocene climate cycles on the edge of the Zhuye Lake (Chen *et al*., 2001; Jin *et al*., 2004), but sediments from different locations of the lake may have variable responses to climate cycles (Li *et al*., 2011). In this paper, we investigated the climate cycles implied by the sediments in the central part of the Zhuye Lake. The grain-size, total organic carbon content (TOC), C/N and $\delta^{13}C$ data from the QTH01 and QTH02 sections are analyzed by wavelet analysis for further investigating the Holocene climate cycles in different parts of the lake and in the marginal region of the Asian monsoon.

2 Study Area

The Zhuye Lake (38º50′–39º15′N, 103º20′–104º10′E) is the terminal lake of the Shiyang River drainage basin (Fig. 1). The Shiyang River drainage basin (37º02′–39º17′N, 100º57′–104º57′E) is located in the eastern part of Hexi Corridor in Gansu Province, China. It is bounded in the south by the foothills of the Qilian Mountain. The peak of the Qilian Mountain is over 5000 m a.s.l.). The Shiyang River flows 300 km from the Qilian Mountain in the south to the Tengger Desert in the north. The Shiyang River drainage basin has a catchment area of 41 600 km^2, and crosses three climate zones. The mean annual temperature in the Qilian Mountain is 2–4℃ and the annual precipitation is 200–700 mm. In the middle and lower reaches of the Shiyang River, the mean annual temperature is 6–8℃ and the annual precipitation is 50–200 mm. Around the terminal lake area, the annual evaporation capacity exceeds 2600 mm (Chen and Qu, 1992). Due to the diversion of water

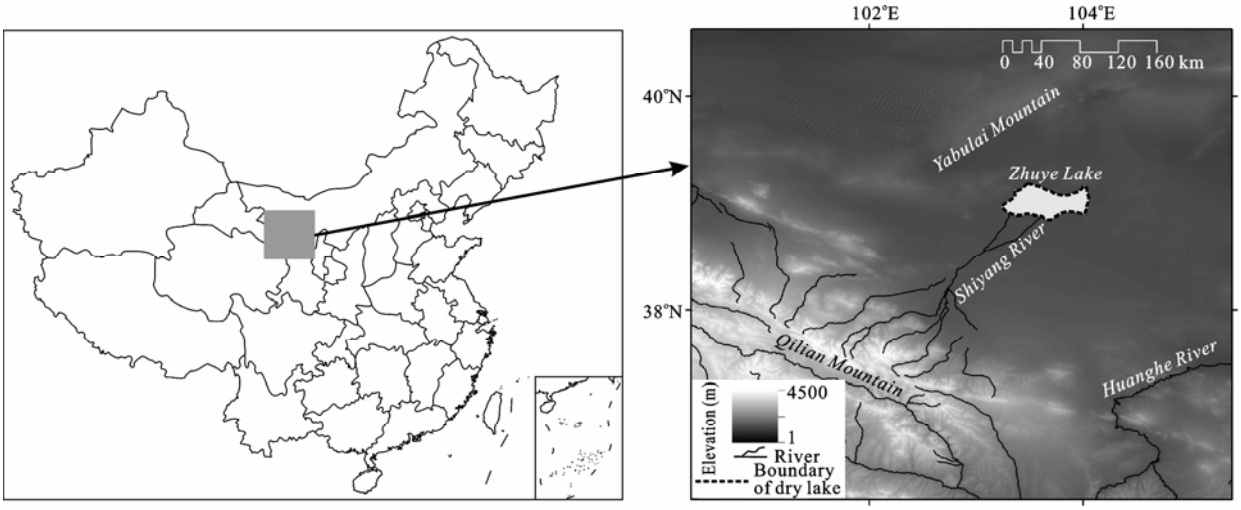

Fig. 1 Location of study area

from the Shiyang River for irrigation, the Zhuye Lake has been dried up since the 1960s. At present, the dry lakes exist in several depressions on the Tengger Desert margins, and only fill with water in years with sufficient precipitation. However, these are the remnants of a single lake of more than 500 km^2 that survived even into historic times (Pachur *et al*., 1995; Zhang *et al*., 2004), and during the past 2000 years the lake-level fell and the lake was divided into smaller lakes (Feng, 1963; Li, 1993).

3 Materials and Methods

We hand-excavated two sections, QTH01 and QTH02, in the central part of the Zhuye Lake (Fig. 1) (1309 m a.s.l.). QTH01, measuring 250 cm × 150 cm, was taken to a depth of 692 cm; QTH02, measuring 300 cm × 150 cm, was taken to 736 cm (Fig. 2). Stratigraphically, at 0–165 cm, QTH01 is composed of yellow and brownish clay and sandy clay deposits, influenced by human activities on the top of the section; at 165–230 cm, it is light red silty clay with many brown spots; at 230–315 cm, it is silty peat with plant fragments and mollusk shells; at 315–450 cm, it is a typical lacustrine deposit with grey silt, clayey silt and carbonate; at 450–495 cm, it is a grey sand layer with some cracked mollusc shells; at 495–603 cm, it is a lacustrine deposit with grey, carbonate enriched silt; at 603–692 cm, it is grey or yellow sand and well sorted (Fig. 3). QTH02 shows a similar stratigraphy. QTH01 was sampled at 2 cm intervals at the lake sediment layers and at 5 cm intervals otherwise, yielding 292 samples for analyses of grain-size, TOC, δ^{13}C, and C/N ratios. QTH02 was sampled at 2 cm intervals, yielding 368 samples for analysis of grain-size. The Sanjiaocheng section is located in the west margin of the lake (39°00′38″N, 103°20′25″E), at the elevation of 1320 m a.s.l. (Fig. 2), and the lithology has been described by Chen *et al*. (2001).

3.1 Chronology

Six Accelerator Mass Spectrometry (AMS)-radiocarbon dates (Beijing University Dating Laboratory) and eight conventional radiocarbon dates (Lanzhou University Dating Laboratory) were obtained from the bulk sediments and shells. Dates were calibrated by using CALIB 5.01 and were reported in calibrated years (Reimer *et al*., 2004). Of the 14 radiocarbon dates, 11 were from QTH01, the remainder from QTH02 (Table 1). For correcting the hard water effects, six optically stimulated luminescence (OSL) samples were dated to provide chronological control at QTH01 section. Long *et al*. (2010) have reported the six OSL dates (Fig. 3; Table 2). Quartz (38–63 μm) OSL measurements are performed in the Luminescence Dating Laboratory of the Qinghai Institute of Salt Lakes, Chinese Academic Sciences, by using an automated Risø TL/OSL-20 reader (Risø DTU, Denmark). OSL dating procedures referred the method in Lai and Wintle (2006). The OSL and ^{14}C ages are in good agreement, suggesting that the established chronology is robust. In addition, as shown in Table 1, the radiocarbon age difference of the organic matter and the shells at the depth of 315 cm is 30 years. Generally, the

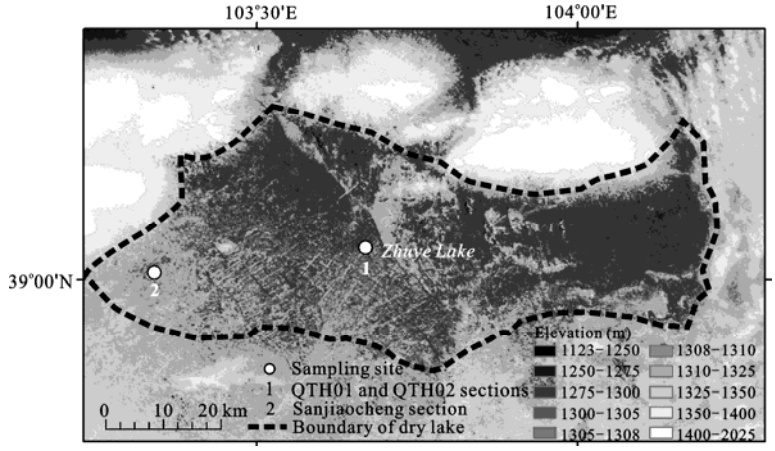

Elevation data are based on the ASTER-GDEM dataset, with 30 m resolution, and downloaded from https://wist.echo.nasa.gov/wist-bin/api/ims.cgi?mode=MAINSRCH&JS=1

Fig. 2 Sampling sites in Zhuye Lake

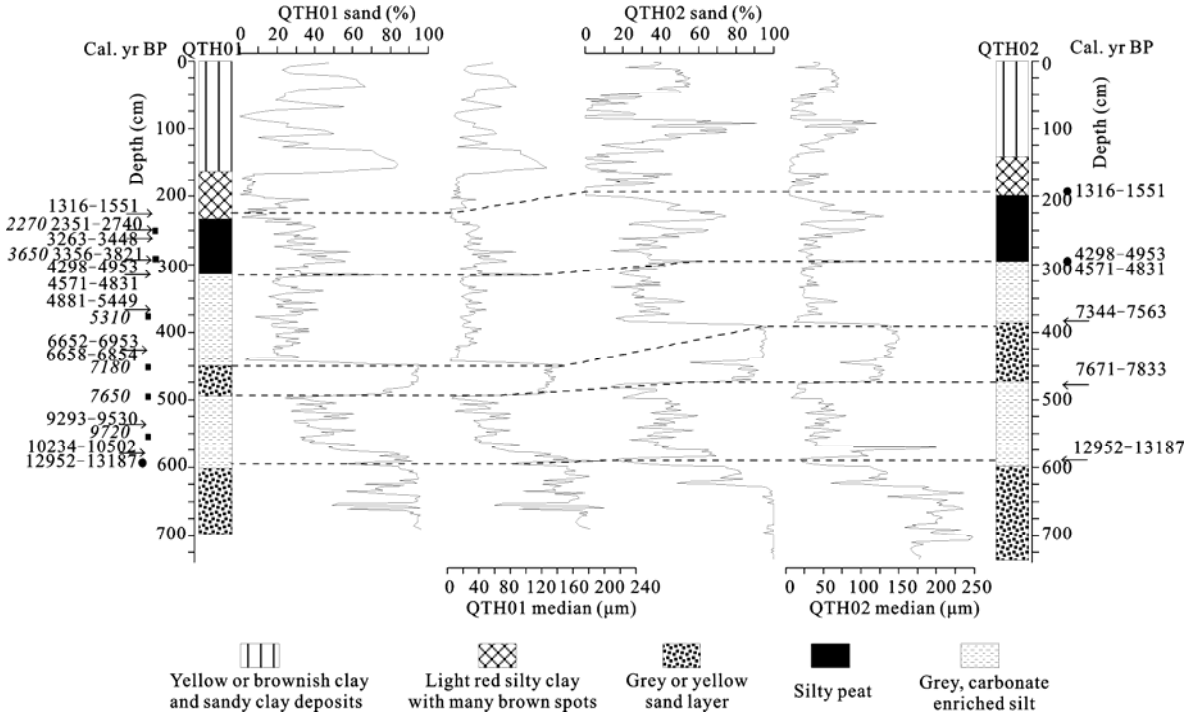

Subsurface correlation of QTH01 and QTH02 sections is based on the grain-size data (sand (%) and median (μm)) plotted against depth. The arrowheads show the radiocarbon dates, and the black rectangles show the optically stimulated luminescence (OSL) dates. The OSL dates are highlighted by italics. Based on the correlation of the grain-size data and lithology, we extrapolate three radiocarbon dates between the two sections. The extrapolated dates are marked with black circles

Fig. 3 Lithology and dates in QTH01 and QTH02 sections

Table 1 Accelerator Mass Spectrometry and conventional radiocarbon dates at QTH01 and QTH02 sections

Laboratory number	Section	Depth in core (cm)	Dating material	$\delta^{13}C$ (%)	^{14}C age (yr BP)	Calibrated ^{14}C age (2σ) (cal. yr BP)
LUG96-44	QTH01	2.25	Organic matter	–27.8	1550±60	1316–1551
LUG96-45	QTH01	2.50	Organic matter	–28.2	2470±90	2351–2740
BA05223	QTH01	2.62	Shells		3140±40 (AMS)	3263–3448
LUG96-46	QTH01	2.90	Organic matter	–28.5	3300±90	3356–3821
LUG96-47	QTH01	3.15	Organic matter	–27.4	4130±110	4298–4953
BA05224	QTH01	3.15	Shells		4160±40 (AMS)	4571–4831
LUG96-48	QTH01	3.60	Organic matter	–25.7	4530±80	4881–5449
LUG96-49	QTH01	4.25	Inorganic matter		5960±65	6652–6953
BA05225	QTH01	4.25	Shells		5920±40 (AMS)	6658–6854
LUG02-25	QTH01	5.37	Organic matter	–24.3	8412±62	9293–9530
LUG02-23	QTH01	5.72	Organic matter	–24.7	9183±60	10234–10502
BA05222	QTH02	3.88	Shells		6550±40 (AMS)	7344–7563
BA05221	QTH02	4.75	Shells		6910±40 (AMS)	7671–7833
BA05218	QTH02	5.91	Shells		11175±50 (AMS)	12952–13187

organic matter is less influenced by hard water effects than shells (inorganic matter). Based on these results, we conclude that the hard water effects are slight in the sections. Most stratigraphic units are correlated between the two sections. After analyzing lithology and grain-size, three dates were extrapolated between the QTH01 and QTH02 sections (Fig. 3). The ages of sampled horizons were derived by linear interpolating between the dates.

3.2 Grain-size

Grain-size distribution was determined by using a Mastersizer 2000 particle analyzer (Malvern Instruments, Britain), which automatically yields the percentages of

Table 2 Optically stimulated luminescence ages for six samples at QTH01 section

Depth (cm)	U (ppm)	Th (ppm)	K (%)	Water content (%)	Dose rate (Gy/kyr)	De (Gy)	Age (kyr)
250	11.19±0.35	2.65±0.16	0.58±0.03	50±5	2.02±0.16	4.70±0.10	2.27±0.19
290	6.27±0.27	4.34±0.20	0.97±0.04	45±5	1.76±0.13	6.50±0.20	3.65±0.30
375	4.08±0.21	1.70±0.14	0.32±0.02	58±5	0.76±0.07	4.10±0.30	5.31±0.60
455	4.47±0.23	2.93±0.18	1.30±0.05	44±5	1.60±0.12	11.80±0.50	7.18±0.63
495	8.10±0.28	2.82±0.17	0.97±0.03	57±5	1.49±0.12	11.50±0.30	7.65±0.67
560	10.65±0.35	5.48±0.25	1.17±0.04	51±5	2.21±0.18	21.60±0.50	9.72±0.81

Note: All the optically stimulated luminescence dates were adjusted to AD 1950 to compare with calibrated ^{14}C ages
Source: Long *et al*. (2010)

clay-, silt- and sand-size fractions, as well as median, mean and mode sample diameters. The sediment (0.2–0.4 g) was pretreated by heating in 10 mL of 10% H_2O_2 to remove organics, heating in 10 mL 10% HCl to remove carbonate that otherwise would bond different mineral fractions, then shaking in Na-hexametaphosphate to disaggregate the sediment for 1 h prior to analysis. In different time scales, grain-size of lake sediments indicates variable climatic information. In interannual scale, coarse lake sediments can be related with basin-wide high precipitation and runoff, and in centennial and millennial scale, it is described as the sediment sorting principle that the grain-size of lake sediments becomes finer and finer from the shore to the center, and sediment belts of different grain-size fractions levels can be distinguished, as a result, the grain-size of lake sediments is in close relation to water level and the energy of the inflows (Lerman, 1978; Chen *et al*., 2003).

3.3 TOC, C/N and $\delta^{13}C$

Percent total nitrogen N (%) and percent organic carbon C (%) were measured by vario EL III Element Analyzer (Elementar, Germanry). Sediment (5 g) was pretreated with 18% HCl for 24 h at room temperature to remove inorganic carbonate. Molar ratios were then determined by using atomic weights (C_{org} / N_{total} = (C (%) / 12.01) / (N (%) / 14.002)). The $\delta^{13}C$ value of organic matter was measured by using a MAT-252 mass spectrometer (Thermo Electron Corporation, USA). The samples were dried in oven under 60℃, and then grounded to about 1.25 mm in size. The pretreated samples were combusted with oxygen gas and converted to CO_2 gas in a high-vacuum system. The CO_2 gas was then purified, collected and measured on the MAT-252 mass spectrometer with carbon isotope error being less than 0.1‰. All isotopic values were reported in the standard δ-notation in permil relative to V-PDB. Percent TOC values reflect the amount of organic matter produced within a lake basin, as well as terrestrial organic matter washed in from its watershed (Dean, 1999; Meyers and Lallier-Vergas, 1999). C/N values reflect the ratio of aquatic organic matter to terrestrial organic matter (Meyers and Lallier-Vergas, 1999; Talbot and Laerdal, 2000). The photosynthetic plants incorporate carbon into organic matter using the C3 Calvin pathway, C4 Hatch-Slack pathway, and CAM pathway (O′Leary, 1988). Organic matter produced from atmospheric CO_2 by plants using the C3 pathway has an average $\delta^{13}C$ (PDB) value of ca. –28‰ (–34‰ to –23‰), by those using the C4 pathway ca. –14‰ (–22‰ to –6‰) and by those using CAM pathway between –20‰ and –10‰ (O′Leary, 1988).

3.4 Wavelet analysis

Many time series in climatology exhibit non-stationarity in their statistics. Wavelet analysis attempts to calculate dominant periodic signals by decomposing a time series into time/frequency space simultaneously. Wavelet analysis was carried out to the samples between 2.25 m and 5.99 m in the QTH01 section (13079–1447 cal. yr BP), and between 1.95 m and 5.91 m in the QTH02 section (13079–1447 cal. yr BP). At the bottom and top parts of the two sections, there were no dates to control the chronology. In the sections of QTH01 and QTH02, the time series were unevenly spaced in time, thus requiring a kind of interpolation before wavelet analysis could be performed. The cubic spline function was used to interpolate all the time series and proxies into equally spaced series, with a resolution of 30 years. In this study, we used the wavelet analysis introduced by Torrence and Compo (1998).

4 Results

4.1 Grain-size

Interpolated by the cubic spline function with a resolution of 30 years, the percentage of sand content and median grain-size curves of the QTH01 and QTH02 sections are shown in Fig. 4. The wavelet power spectrum and global wavelet power spectrum show clear cycles for the grain-size changes in the two sections (Fig. 5). For the percentage of sand content in the QTH01 section, the ~128– ~1024-year cycle is obvious, and the peaks are at ~256-year and ~1024-year, both of which can pass the 99% significance level. The median grain-size of QTH01 shows apparent cycles between ~128– ~1024-year, and the peak is at ~256-year, which is significant at 99% level. The cone of influence (COI) is the region of the wavelet spectrum in which edge effects become important. Most of the ~4000-year cycle indicated by the sand content and median grain-size in the QTH01 section is in the cross-hatched region (the cone of influence); therefore, the ~4000-year cycle can be ignored. In the QTH02 section, as shown by the percentage of sand content, the ~128– ~2048-year cycle is obvious, and the peak is at ~512-year. The median grain-size of the QTH02 section shows ~512 and ~2048-year, two obvious cycles, however, some part of the ~2048-year cycle, especially the obvious part showing the ~2048-year cycle, is in the cross-hatched region (the cone of influence).

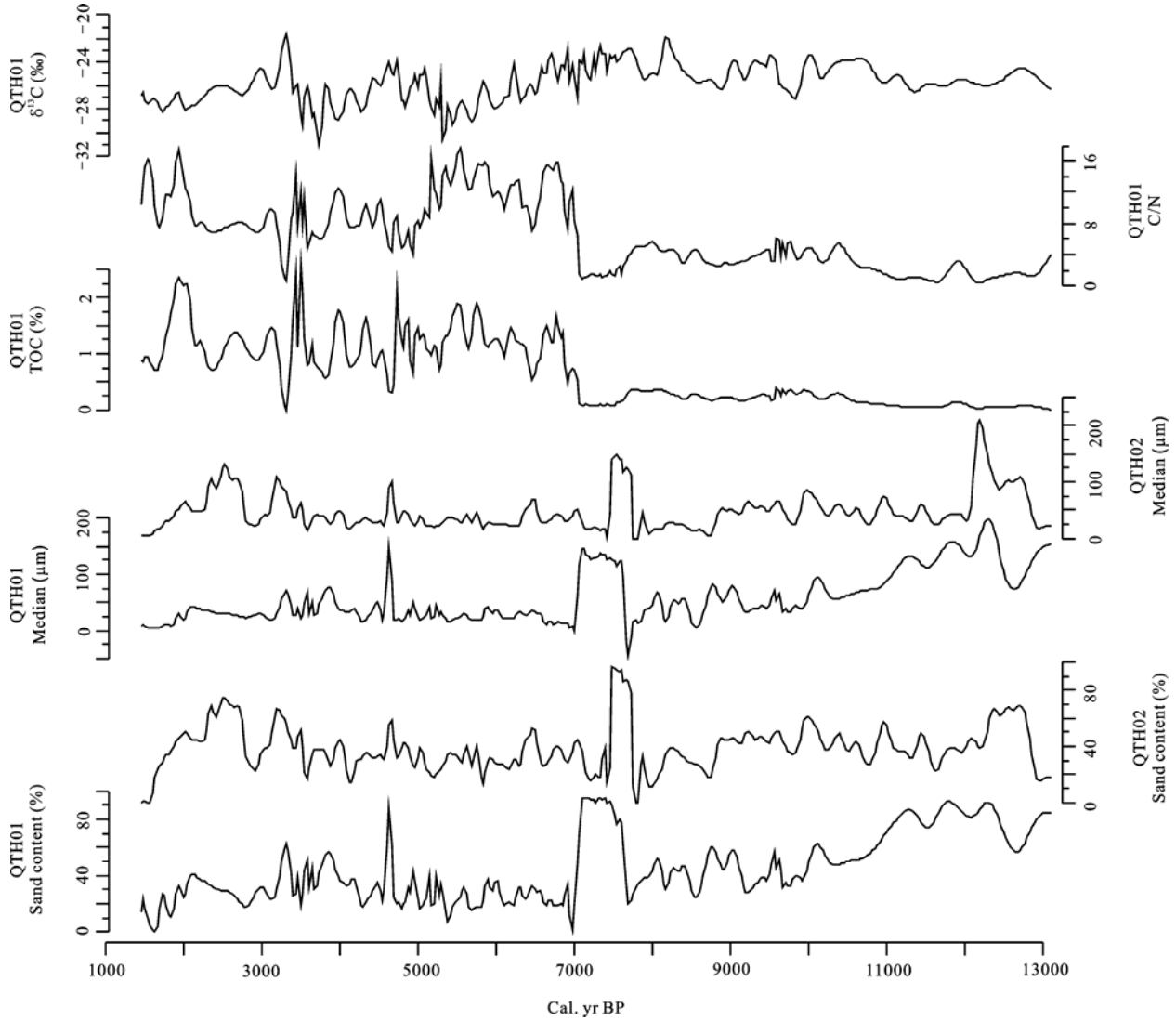

Data are interpolated into equally spaced series using the cubic spline function, with a resolution of 30 years

Fig. 4 Time series and proxies′ values

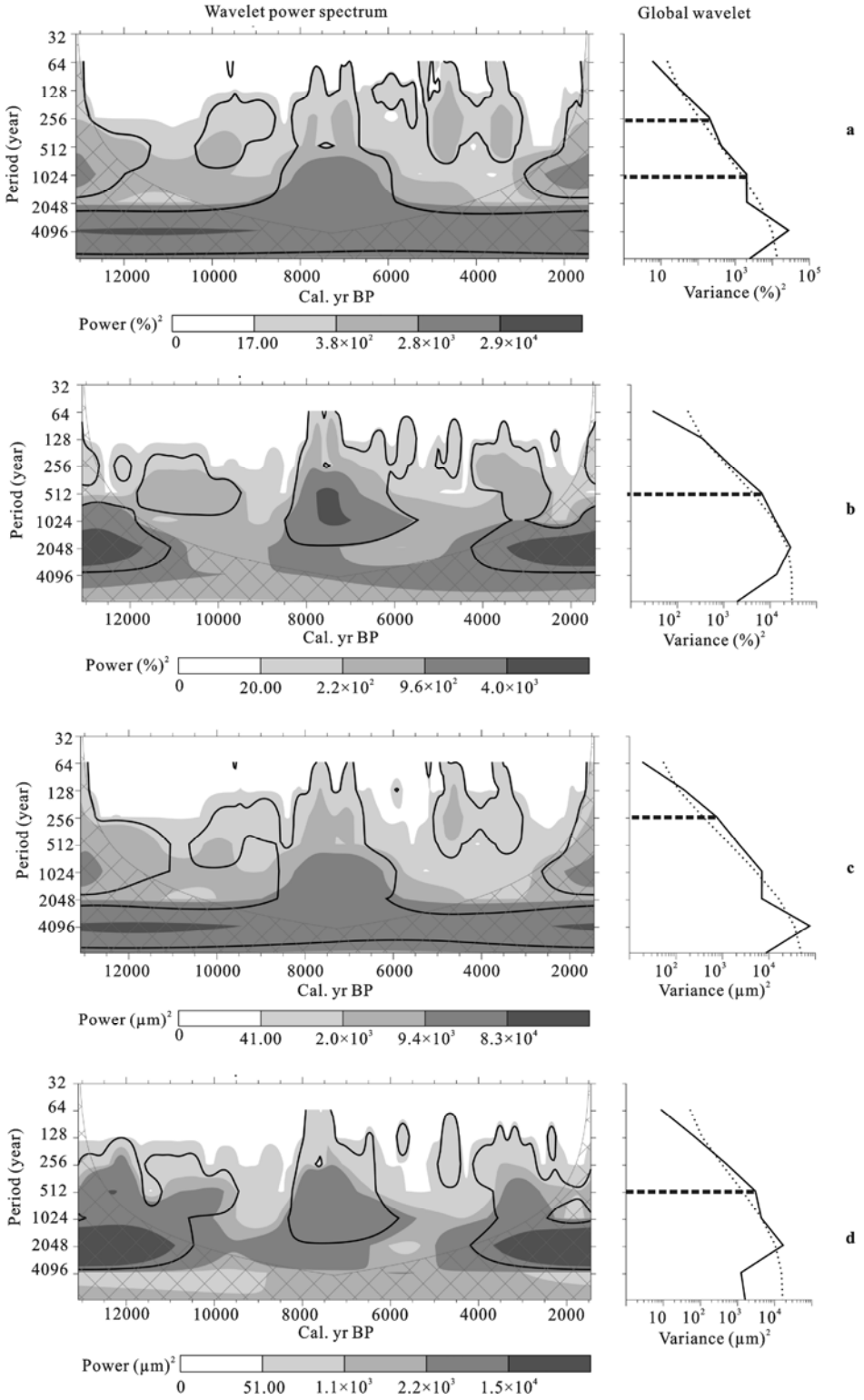

The contour levels are chosen so that 75%, 50%, 25%, and 5% of the wavelet power is above each level, respectively. The cone of influence, which can reduce the degree of variation, is manifest in the cross-hatched region. Black contour is the 99% significance level, using a red-noise (autoregressive lag1) background spectrum. Black line is the global wavelet power spectrum; dashed line is the significance for the global wavelet spectrum, with the 99% significance level; and straight broken lines indicate the peaks of cycles

a, percentage of sand content in QTH01 (%); b, percentage of sand content in QTH02 (%); c, value of median grain-size in QTH01 (μm); d, value of median grain-size in QTH02 (μm)

Fig. 5 Wavelet power spectrum

Therefore, the ~2048-year cycle can be ignored.

4.2 TOC, C/N and $\delta^{13}C$

Interpolated by the cubic spline function with a resolution of 30 years, the TOC, C/N and $\delta^{13}C$ curves at the QTH01 section are shown in Fig. 4. The wavelet power spectrum and global wavelet power spectrum show clear cycles for the change of TOC, C/N and $\delta^{13}C$ (Fig. 6). For the percentage of TOC, the ~128-year– ~512-year cycle is obvious, the peak is around 256-year, and these cycles are significant at 99% level. According to the wavelet power spectrum, the ~256-year cycle is more obvious during the mid to late Holocene (~7.5 cal. kyr BP– ~1.5 cal. kyr BP) than the early Holocene. Most of the ~4000-year cycle is in the cross-hatched region (the cone of influence); therefore, the ~4000-year cycle can be ignored. The values of C/N show obvious ~512-year cycle, which is significant at 99% level, and the 4000-year cycle also can be ignored because of the cone of influence. The ~512-year cycle is also more obvious during the mid to late Holocene than the early Holocene. The $\delta^{13}C$ values show obvious ~256-year cycle, which is significant at 99% level. The ~256-year cycle from $\delta^{13}C$ is obvious since the early Holocene (~10.5 cal. kyr BP). The ~2048– ~4096-year cycle also can be detected; however, most of the cycle, especially the part showing the ~2048– ~4096-year cycle, is in the cross-hatched region; therefore, the result can be ignored. From the organic geochemical proxies, the ~128– ~512-year cycle can be detected, and the peaks are at ~256-year and ~512-year. Compared with the early Holocene, the values of TOC and C/N are more sensitive to climate cycles during the mid to late Holocene. As shown in Fig. 4, the TOC and C/N values are very low during the early Holocene, so the climate cycles can not be detected accurately. The cycles indicated by $\delta^{13}C$ values are obvious since ~10.5 cal. kyr BP, which might be influenced by low TOC. However, the climate cycles indicated by grain-size can be detected over the entire Holocene. The low contents of organic matter could make the low sensitivities of TOC, C/N and $\delta^{13}C$ to climate cycles.

5 Discussion

In arid region, effective moisture is one of the most important limiting factors for plant growth, therefore, the climate cycles shown by TOC, C/N and $\delta^{13}C$ are primarily related to the basin-wide effective moisture changes. Grain-size of lake sediments is complicated, which may be related with the lake-level, precipitation, hydrodynamic conditions, *etc*. In the QTH01 and QTH02 sections, the grain-size shows obvious ~256-year, ~512-year and ~1024-year cycles, at the same time, the TOC, C/N and $\delta^{13}C$ also demonstrate obvious ~256-year and ~512-year cycles. Long-term grain-size change for lake sediments could be affected by lake-level change that is essentially correlated with the basin-wide effective moisture change. The results of consistent climate cycles show that the grain-size can be linked to the geochemical proxies by effective moisture change. Every proxy has its own sensitivity to climate change, thus different climate cycles can be reflected by different proxies. Totally, the ~256-year, ~512-year and ~1024-year cycles are the obvious climate cycles illustrated by the proxies from the QTH01 and QTH02 sections (Table 3).

Chen *et al*. (2001) and Jin *et al*. (2004) reported millennial and centennial scale climate cycles, at the Sanjiaocheng section (Fig. 2), and detailed results from the power spectrum analysis of TOC and the percentage of the conifer tree showed a series of millennial and centennial scale changes, with cycles of 1553-year, 1506-year, 1190-year, 686-year, 617-year, 504-year, 314-year, 180-year and 131-year, especially the 1553-year cycle corresponding to seven times of dry-wet intervals during the Holocene. The Sanjiaocheng section is a well-dated section, and the hard water effect is around 550-year. The slight hard water effect has few effects on studying Holocene millennial scale climate change (Chen *et al*., 2001). In this study, the comparison between OSL and radiocarbon dates also proves the negligible hard water effect. Therefore, the dating error can not account for the different climate cycles in the same lake. According to the topography of the lake basin (Fig. 2), the QTH01 and QTH02 sections are located in the central part of the lake basin, at the elevation of 1309 m a.s.l. The Sanjiaocheng section is located in the west margin of the lake basin, at the elevation of 1320 m a.s.l. During the Holocene epoch, the elevation difference between the Sanjiaocheng section and the QTH01 and QTH02 sections is ~10 m. In different locations of the lake basin, sediments might have variable responses to climate cycles. Therefore, the topography could be the key factor for the different climate cycles.

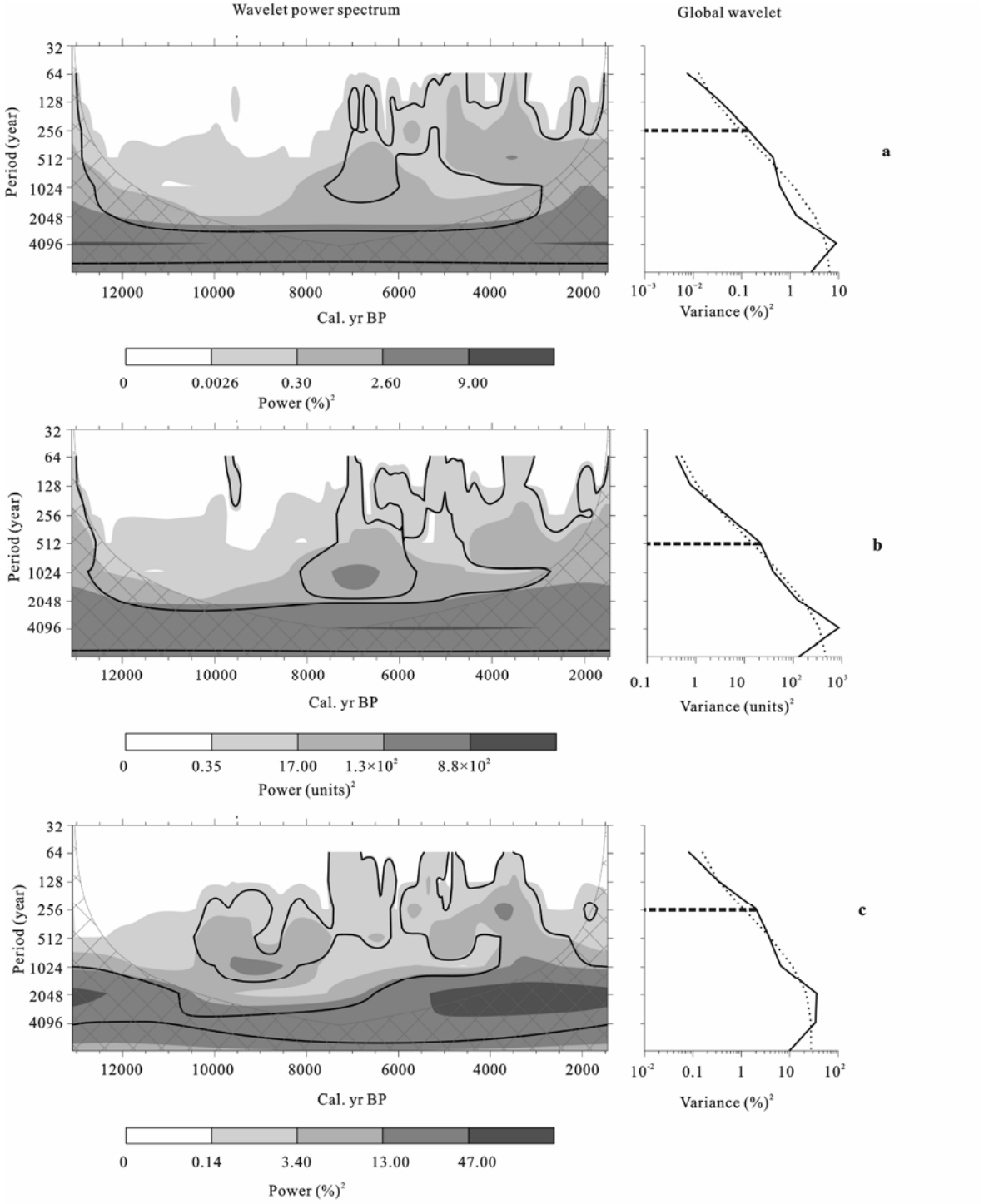

The contour levels are chosen so that 75%, 50%, 25%, and 5% of the wavelet power is above each level, respectively.
The cone of influence, which can reduce the degree of variation, is manifest in the cross-hatched region.
Black contour is the 99% significance level, using a red-noise (autoregressive lag1) background spectrum.
Black line is the global wavelet power spectrum; dashed line is the significance
for the global wavelet spectrum, with the 99% significance level;
and the straight broken lines indicate the peaks of cycles
a, TOC (%); b, C/N; c, $\delta^{13}C$ (‰)

Fig. 6 Wavelet power spectrum in QTH01

Table 3 Main climate cycles implied by wavelet analysis for sand content, grain-size median, TOC, C/N and $\delta^{13}C$ (years)

Section	Sand content	Median	TOC	C/N	$\delta^{13}C$
QTH01	~256, ~1024	~256	~128– ~512	~512	~256
QTH02	~512	~512	–	–	–

Note: All the listed climate cycles are significant at 0.01 level

In the Asian monsoon domain, the Holocene stalagmite record obviously showed ~240-year cycle in Oman (Fleitmann *et al*., 2003). In the southern China, the power spectral analysis of the $\delta^{18}O$ record from Dongge Cave indicated statistically significant centennial periodicities centered on 558-year, 206-year, and 159-year (Wang *et al*., 2005). Beside the Holocene stalagmite records, according to the power spectral analysis, the 1140-year, 490-year, 250-year and 220-year climate cycles can be detected during the Holocene in Huguangyan Maar Lake, southern China (Liu *et al*., 2000). In the low-latitude regions, the Holocene centennial scale climate cycles are close to significant periods of the $\delta^{14}C$ record that are linked to solar radiation or the solar-induced climate change amplified by salinity effects on North Atlantic thermohaline circulation (Stuiver and Braziunas, 1993).

In mid-latitude China, the peat record from the northeast of the Qinghai-Tibet Plateau indicated the 1428-year, 512-year, 255-year and 217-year climate cycles by spectral analysis (Xian *et al*., 2006), and in the similar area, Hong *et al*., (2003) investigated the correlation between the Holocene Indian summer monsoon and the North Atlantic ice-rafting events. In the Hexi Corridor, the persistent millennial scale climate variability was found to be linked to the North Atlantic ice-rafting events (Yu *et al*., 2006). According to the climate cycles reconstructed by the sediments from the Zhuye Lake, the Holocene millennial and centennial scale climate cycles are notable in the northwest margin of the Asian monsoon (Chen *et al*., 2001; Jin *et al*., 2004). These climate cycles can be influenced by the Asian summer monsoon variability from the low-latitude regions. Furthermore, the Holocene North Atlantic ice-rafting events can have some effects on the northwest margin of the Asian summer monsoon.

6 Conclusions

This study investigated the Holocene climate cycles in the northwest margin of the Asian monsoon. According to 14 ^{14}C dates and 6 OSL dates, the QTH01 and QTH02 sections, in the central part of the Zhuye Lake, provided high-resolution Holocene climate records that are ideal for climate cycle study. Based on the wavelet analysis for the grain-size, TOC, C/N and $\delta^{13}C$ data, the ~256-year, ~512-year and ~1024-year climate cycles could be detected in the sediments of the Zhuye Lake. However, these cycles are different from the previous studies from the Sanjiaocheng section on the edge of the lake. In different locations of the lake, the sediments have variable responses to climate changes. In the mid-latitude regions of China, the Holocene climate cycles are relatively consistent with the cycles from the low latitude regions due to the advance and retreat of the Asian monsoon. In addition, the North Atlantic ice-rafting events have some effects on the Holocene climate cycles in the northwest margin of the Asian monsoon. However, in the study area, the mechanism for the Holocene Asian monsoon impacts is still unclear, and quantitative climate change reconstruction and climate models are needed for the further exploration of the climate system.

Acknowledgements

We thank Dr. Hao Long, who was of great assistance with OSL dating. We also thank Dr. Cheng Hongyi and Dr. Qiang Zhao for their help with field and laboratory work. Thanks are extended to Mr. Steven Grey for his assistance in checking the English of this paper.

References

Bond G, Showers W, Cheseby M *et al*., 1997. A pervasive millennial-scale cycle in North Atlantic Holocene and Glacial Climates. *Science*, 278(5341): 1257–1266. doi: 10.1126/science.278.5341.1257

Bond G, Kromer B, Beer J *et al*., 2001. Persistent solar influence on North Atlantic Climate during the Holocene. *Science*, 294(5549): 2130–2136. doi: 10.1126/science.1065680

Chen Jingan, Wan Guojiang, Zhang Dian *et al*., 2003. Environmental records of different time scales in lake-sediments: Grain-size of sediments. *Science in China* (*Series D*), 33(6): 563–568. (in Chinese)

Chen Longheng, Qu Yaoguang, 1992. *Water-land Resources and Reasonable Development and Utilization in the Hexi Region*. Beijing: Science Press. (in Chinese)

Chen F, Zhu Y, Li J *et al*., 2001. Abrupt Holocene changes of the

Asian monsoon at millennial- and centennial-scales: Evidence from lake sediment document in Minqin Basin, NW China. *Chinese Science Bulletin*, 46(23): 1942–1947. doi: 10.1360/03 wd0245

Dansgaard W, Johnsen S J, Clausen H B *et al*., 1993. Evidence for general instability of past climate from a 250-kyr ice-core record. *Nature*, 364(6434): 218–220. doi: 10.1038/364218a0

Dean W E, 1999. The carbon cycle and biogeochemical dynamics in lake sediments. *Journal of Paleolimnology*, 21(4): 375–393. doi: 10.1023/A:1008066118210

Fleitmann D, Burns S J, Mudelsee M *et al*., 2003. Holocene forcing of the Indian monsoon recorded in a stalagmite from southern Oman. *Science*, 300(5626): 1737–1739. doi: 10.1126/ science.1083130

Feng S H, Kaufman D, Yoneji S *et al*., 2003. Cyclic variation and solar forcing of Holocene Climate in the Alaskan Subarctic. *Science*, 301(5641): 1890–1893. doi: 10.1126/science.1088568

Feng Shengwu, 1963. The evolution of the drainage system of the Minqin oasis. *Acat Geographica Sinica*, 29(3): 241–249. (in Chinese)

Grootes P M, Stuiver M, White J W C *et al*., 1993. Comparison of oxygen isotope records from the GISP2 and GRIP Greenland ice cores. *Nature*, 366(6455): 552–554. doi: 10.1038/366552a0

Gupta A K, Anderson D M, Overpeck J T, 2003. Abrupt changes in the Asian southwest monsoon during the Holocene and their links to the North Atlantic Ocean. *Nature*, 421(6921): 354–357. doi: 10.1038/nature01340

Hong Y T, Hong B, Lin Q H *et al*., 2003. Correlation between Indian Ocean summer monsoon and North Atlantic climate during the Holocene. *Earth Planet Science Letters*, 211(3–4): 371–380. doi: 10.1016/S0012-821X(03) 00207-3

Jin Liya, Chen Fahu, Zhu Yan, 2004. Holocene climatic periodicities recorded from lake sediments in the arid-semiarid areas of northwestern China. *Marine Geology & Quaternary Geology*, 24(2): 101–108. (in Chinese)

Lai Z P, Wintle A G, 2006. Locating the boundary between the Pleistocene and the Holocene in Chinese loess using luminescence. *The Holocene*, 16(6): 893–899. doi: 10.1191/ 0959683606 hol980rr

Lerman A, 1978. *Lake*: *Chemistry*, *Geology*, *Physics*. Berlin: Springer-Verlag.

Li Bingcheng, 1993. A study on the Zhuye Lake and its historical evolution. *Acta Geographica Sinica*, 48(1): 55–60. (in Chinese)

Li Y, Wang N, Cheng H *et al*., 2009a. Holocene environmental change in the marginal area of the Asian monsoon: A record from Zhuye Lake, NW China. *Boreas*, 38(2): 349–361. doi: 10.1111/j.1502-3885.2008.00063.x

Li Y, Wang N, Morrill C *et al*., 2009b. Environmental change implied by the relationship between pollen assemblages and grain-size in NW Chinese lake sediments since the Late Glacial. *Review of Palaeobotany and Palynology*, 154(1–4): 54–64. doi: 10.1016/j.revpalbo.2008.12.005

Li Y, Wang N, Li Z *et al*., 2011. Holocene palynological records and their responses to the controversies of climate system in the Shiyang River drainage basin. *Chinese Science Bulletin*, 56(6): 535–546. doi: 10.1007/s11434-010-4277-y

Liu J Q, Lu H Y, Negendank J *et al*., 2000. Periodicity of Holocene climatic variations in the Huguangyan Maar Lake. *Chinese Science Bulletin*, 45(18): 1712–1717. doi: 10.1007/s11434-009-0585- 5

Long H, Lai Z, Wang N *et al*., 2010. Holocene climate variations from Zhuyeze terminal lake records in East Asian monsoon margin in aridnorthern China. *Quaternary Research*, 74(1): 46–56. doi: 10.1016/j.quageo.2009.05.005

Meyers P A, Lallier-Vergas E, 1999. Lacustrine sedimentary organic matter records of late Quaternary paleoclimates. *Journal of Paleolimnology*, 21(3): 345–372. doi: 10.1016/S0031-0182 (02)00591-6

O′Leary M H, 1988. Carbon isotopes in photosynthesis. *Bioscience*, 38(5): 328–336. doi: 10.1029/96GB02345

Pachur H J, Wünnemann B, Zhang H, 1995. Lake evolution in the Tengger Desert, northwestern China, during the last 40 000 Years. *Quaternary Research*, 44(2): 171–180. doi: 10.1006/ qres.1995.1061

Palus M, Kurths J, Schwarz U *et al*., 2007. The solar activity cycle is weakly synchronized with the solar inertial motion. *Physics Letters A*, 365(5–6): 421–428. doi: 10.1016/j.physleta. 2007.01.039

Rahmstorf S, 2003. Timing of abrupt climate change: A precise clock. *Geophysical Research Letter*, 30(10): 1510. doi: 10.1029/ 2003GL017115

Reimer P J, Baillie M G L, Bard E *et al*., 2004. IntCal04 terrestrial radiocarbon age calibration, 0–26 cal. kyr BP. *Radiocarbon*, 46(3): 1029–1058. doi: 10.1016/ S0025-3227(97)00107-2

Sonett C P, Suess H E, 1984. Correlation of bristlecone pine ring width with atmospheric ^{14}C variations. *Nature*, 307(5947): 141–142. doi: 10.1038/307141a0

Stuiver M, Braziunas T, 1993. Sun, ocean, climate and atmospheric $^{14}CO_2$: An evaluation of causal and spectral relationships. *The Holocene*, 3(3): 289–305. doi: 10.1177/095968369300300401

Talbot M R, Laerdal T, 2000. The late Pleistocene-Holocene paleolimnology of Lake Victoria, East Africa, based upon elemental and isotopic analyses of sedimentary organic matter. *Journal of Paleolimnology*, 23(2): 141–164. doi: 10.1016/ S0033-5894(03)00008-5

Torrence C, Compo G P, 1998. A practical guide to wavelet analysis. *Bulletin of American Meteorological Society*, 76(1): 61–78. doi: 10.1175/1520-0477

Xian Feng, Zhou Weijian, Yu Xuefeng *et al*., 2006. Evidence for abrupt changes of the Asian monsoon during the Holocene: From the peat records of Tibetan Plateau. *Marine Geology & Quaternary Geology*, 26(5): 41–45. (in Chinese)

Wang Y, Cheng H, Edwards R L *et al*., 2005. The Holocene Asian monsoon: Links to solar changes and North Atlantic climate. *Science*, 308(5723): 854–857. doi: 10.1126/science.1106296

Yiou P, Fuhrer K, Meeker L D *et al*., 1997. Paleoclimate variabil-

ity inferred from the spectral analysis of Greenland and Antarctic ice-core data. *Journal of Geophysical Research*, 102(c12): 26441–26454. doi: 10.1029/97JC00158

Yu Y, Yang T, Li J *et al*., 2006. Millennial-scale Holocene climate variability in the NW China drylands and links to the tropical Pacific and the North Atlantic. *Palaeogeography*, *Palaeoclimatology*, *Palaeoecology*, 233(1–2): 149–162. doi: 10.1016/j.palaeo.2005.09.008

Zhang H C, Peng J L, Ma Y Z *et al*., 2004. Late Quaternary palaeolake levels in Tengger Desert, NW China. *Palaeogeography*, *Palaeoclimatology*, *Palaeoecology*, 211(1): 45–58. doi: 10.1016/j.palaeo.2004.04.006